A Modeling Study of the Impact of Tropical Instability Waves on the Heat Budget of the Eastern Equatorial Pacific

CHRISTOPHE E. R. MENKES AND JÉRÔME G. VIALARD
LODYC (IRD/CNRS/UPMC/MNHN), Paris, France

SEAN C. KENNAN
Oceanographic Center, Nova Southeastern University, Dania Beach, Florida

JEAN-PHILIPPE BOULANGER AND GURVAN V. MADEC
LODYC (IRD/CNRS/UPMC/MNHN), Paris, France

(Manuscript received 30 November 2004, in final form 24 October 2005)

ABSTRACT

A numerical simulation is used to investigate the mixed layer heat balance of the tropical Pacific Ocean including the equatorial cold tongue and the region of vortices associated with tropical instability waves (TIWs). The study is motivated by a need to quantify the effects that TIWs have on the climatological heat budget of the cold tongue mixed layer; there has been some discrepancy between observations indicating very large equatorward heat transport by TIWs and models that disagree on the full three-dimensional budget. Validation of the model reveals that the TIW-induced circulation patterns are realistic but may have amplitudes about 15% weaker than those in the observations. The SST budget within tropical instabilities is first examined in a frame of reference moving with the associated tropical instability vortices (TIVs). Zonal advection of temperature anomalies and meridional advection of temperature by current anomalies dominate horizontal advection. These effects strongly heat the cold cusps and slightly cool the downwelling areas located at the leading edge of the vortices. Cooling by vertical mixing is structured at the vortex scale and almost compensates for horizontal advective heating in the cold cusps. In contrast to some previous studies, TIW-induced vertical advection is found to be negligible in the SST budget. Cooling by this term is only significant below the mixed layer. The effect of TIWs on the climatological heat budget is then investigated for the region bounded by 2°S–6°N, 160°–90°W, where instabilities are most active. TIW-induced horizontal advection leads to a warming of 0.84°C month^{-1}, which is of the same order as the 0.77°C month^{-1} warming effect of atmospheric fluxes, while the mean currents and vertical mixing cool the upper ocean by -0.59°C month^{-1} and -1.06°C month^{-1}, respectively. The cooling effect of TIW-induced vertical advection is also negligible in the long-term surface layer heat budget and only becomes significant below the mixed layer. The results above, and in particular the absence of cancellation between horizontal and vertical TIW-induced eddy advection, are robust in three other sensitivity experiments involving different mixing parameterizations and increased vertical resolution.

1. Introduction

Tropical instability waves (TIWs) are common to the Pacific and Atlantic Oceans. They appear in space-borne sea surface temperature (SST) as well as ocean color measurements (Legeckis 1977; Chavez et al. 1999; Chelton et al. 2000; Menkes et al. 2002), as large-scale westward-propagating oscillations of the temperature front separating cold and chlorophyll-rich waters of the equatorial upwelling from warmer and nutrient-depleted waters to the north. These oscillations have a longitudinal scale of 1000–2000 km (Qiao and Weisberg 1995) and propagation speed of about 0.3–0.5 m s^{-1} (Weidman et al. 1999). They are associated with monthly time-scale variations in sea level (Busalacchi et

Corresponding author address: Christophe Eugène Raoul Menkes, LODYC, Case 100, Université Pierre et Marie Curie, 4 Place Jussieu, 75252 Paris Cedex 05, France.
E-mail: menkes@lodyc.jussieu.fr

al. 1994; Perigaud 1990; Weidman et al. 1999), as well as in currents north of the equator. These features can be associated with anticyclonic vortices (Flament et al. 1996; Kennan and Flament 2000; Menkes et al. 2002) as first suggested by Hansen and Paul (1984). At the equator, there is a marked variability in the meridional currents at a 20-day period (Halpern et al. 1988).

TIWs strongly modulate the SST field at the intraseasonal scale and have a complex three-dimensionnal circulation, suggesting a significant impact on the upper-ocean heat balance. Several studies have thus tried to estimate the heat balance within TIWs to understand how the characteristic shape of the TIW is maintained. Observational studies have shown that TIWs induce strong equatorward horizontal heat advection large enough to offset much of the upwelling-induced cooling in the cold tongue (Baturin and Niiler 1997; Kennan and Flament 2000). Moreover, a clear dipole in vertical speed within the vortices associated with TIWs is a persistent feature in both observations and models (Philander et al. 1986; Flament et al. 1996; Menkes et al. 2002). However, because of sampling issues, it has not been possible to accurately infer the vertical heat advection associated with such vortices from observations alone. A modeling study by Jochum et al. (2004) evaluated both meridional and vertical advective heat fluxes associated with TIWs in the Atlantic Ocean in the top 20 m and concluded that there was an almost complete compensation between the meridional heat fluxes and vertical heat fluxes. However, it remains to be determined whether their results hold more generally for the heat budget of the whole mixed layer.

At the seasonal scale, observations by Stevenson and Niiler (1983), Hansen and Paul (1984), Bryden and Brady (1989), Baturin and Niiler (1997), Swenson and Hansen (1999), and Wang and McPhaden (1999) have shown that TIWs play a large role in the cold tongue heat budget. Estimates in those studies suggest that the horizontal TIW flow induces large equatorward transport of heat equivalent or stronger than the effect of the seasonal surface forcing. In these studies based on observations, however, only the horizontal transport of heat by TIWs was quantified and not the vertical component because of data limitations. However, Vialard et al. (2001, hereinafter V01) noted that there might be compensation between the climatological horizontal and vertical eddy heat advection associated with TIWs, although they did not explicitly compute vertical eddy heat advection.

The role of TIWs in the tropical heat budget is thus still an open question. If there is compensation between the horizontal and vertical heat fluxes induced by the TIWs, then their contribution to the long-term budget of the cold tongue might be smaller than what was previously been suggested in observational studies that only took into account horizontal heat flux estimates (Jochum et al. 2004). Vertical advection terms are difficult to estimate from observations, leading us to numerical modeling as a favorable framework for this task.

The goal of this study is to investigate the effect of TIWs on the SST heat budget, at the space and time scales of the waves themselves, as well as their average effect on the cold tongue. In addition, we address the potential compensations between TIW-induced horizontal and vertical advection. We use outputs from a numerical model and separate the heat equation terms into eddy and mean flow components. Section 2 reviews briefly the characteristics of the model and the details of the heat budget analysis. Section 3 provides some validations of TIWs in this model. In section 4, the surface layer heat budget at the space and time scales of TIWs is studied. In section 5, the long-term effect of TIWs on the cold tongue heat budget is revisited, investigating the relative effects of horizontal and vertical advection. Section 6 provides a summary and discussion of the results, including heat budget estimates from sensitivity experiments with different lateral mixing parameterization and increased vertical resolution to illustrate the robustness of our results.

2. The modeling approach

a. Description of the numerical simulation

We use the Laboratoire d'Oceanographie Dynamique et de Climatologie (LODYC) general circulation model (Madec et al. 1999), based on primitive equations, solved by a finite-difference scheme on an Arakawa (1972) C grid. The equation of state is computed from the Jackett and McDougall (1995) formulation. The version used in this study is derived from that described in Maes et al. (1997), Vialard and Delecluse (1998a,b), and Vialard et al. (2001, 2002, 2003). The domain spans the tropical Pacific between 30°N and 30°S and between 120°E and 75°W. The model has 1° zonal resolution and meridional resolution varying from 0.5° between 5°N and 5°S to 2° at the northern and southern boundaries. There are 25 levels (with 10-m resolution down to 150 m and a 1.5-h time step). No-slip boundary conditions and no-flux conditions for heat and salt are applied at the bottom and along the coastlines and boundaries. A damping toward Levitus (1982) monthly temperature and annual salinity values is used near the southern and northern boundaries. In the 20°N–20°S band, no restoring is used in the ocean interior. The turbulent kinetic energy prognostic equa-

tion (Blanke and Delecluse 1993) is used to represent vertical mixing. The lateral mixing for tracers and dynamics acts along isopycnal surfaces as described in Lengaigne et al. (2003).

A combination of *European Remote Sensing Satellites 1* and *2* (*ERS-1* and *-2*) scatterometer-derived wind stresses (Bentamy et al. 1996) and Tropical Atmosphere–Ocean (TAO) array–derived stresses (Menkes et al. 1998) over the 1992–98 period are used to force the ocean model. Heat fluxes are specified from a daily climatology computed from the European Centre for Medium-Range Weather Forecasts (ECMWF) reanalysis (Gibson et al. 1997). The solar heat flux penetrates vertically into the upper ocean. The nonsolar component of the heat flux at the surface is parameterized as the sum of the ECMWF climatology plus a relaxation toward the Reynolds and Smith (1994) SST 1993–96 average seasonal cycle, with a -40 W m^{-2} K^{-1} relaxation coefficient. V01 discuss in detail why this is an acceptable parameterization of the ocean–atmosphere fluxes. The freshwater fluxes are obtained through a combination of the ECMWF reanalysis climatology and interannual anomalies of Global Precipitation Climatology Project (GPCP) rainfall estimates (Huffman et al. 1997). After 3 yr of spinup using climatological winds, the model is run for the 1992–98 period, but results will only be analyzed for 1993–96, a period reasonably representative of the mean seasonal cycle.

The reference experiment used in this study is similar to that of Vialard et al. (2003) except that isopycnal lateral mixing was used instead of horizontal mixing. Orienting the lateral mixing operator along isopycnal surfaces has been shown to improve the representation of the model large-scale circulation fields (Lengaigne et al. 2003). The TIWs themselves did not change dramatically with the introduction of isopycnal mixing, and validations similar to those in Vialard et al. (2003) were done for the present simulation. These validations show that simulated TIWs have a roughly correct level of energy, localization, and seasonality. Their temporal scales, spatial scales, and propagation speeds are also in reasonable agreement with observations. Further validation of TIWs in the present experiment is discussed in section 3 of this paper.

Since the TIW heat budget may be sensitive to the model parameterizations and resolution (Jochum et al. 2005; Pezzi and Richards 2003), we decided to perform several sensitivity experiments. We have performed one sensitivity experiment with isopycnal mixing on tracers and horizontal mixing on momentum and another with horizontal mixing. A third experiment with a tenfold increase in vertical resolution (1 m from the surface to 200 m) has also been performed. The results of these three sensitivity experiments will be discussed in section 6b.

b. Heat budget analysis

The main goal in this study is to investigate the three-dimensional heat balance associated with TIWs, both at intraseasonal and seasonal time scales. In particular, we want to examine the interplay between horizontal and vertical advection due to TIWs. The full three-dimensional temperature equation of the ocean model reads

$$\partial_t T = -u\partial_x T - v\partial_y T - w\partial_z T + D_l(T) + D_z(T) + I(z), \tag{1}$$

where T is the model potential temperature, (u, v, w) are the components of the ocean currents, $D_l(T)$ is the lateral diffusion operator, $D_z(T) = \partial_z(k\partial_z T)$ is the vertical diffusion operator (where k is the vertical diffusion coefficient), and $I(z) = Q_s\partial_z f(z)$ is the heating rate due to the penetrative solar heat flux [Q_S is the net surface solar heat flux and $f(z)$ is the fraction of the solar radiation that reaches depth z].

A proxy for the SST equation is derived by averaging Eq. (1) over the time-varying mixed layer depth h, which reads, as in Vialard and Delecluse (1998a) and Vialard et al. (2001),

$$\begin{aligned}\partial_t \mathrm{SST} = &\underbrace{-\langle u\partial_x T + v\partial_y T + w\partial_z T\rangle}_{\mathrm{A}} + \underbrace{\langle D_l(T)\rangle}_{\mathrm{B}} \\ &\underbrace{-\frac{1}{h}\frac{\partial h}{\partial t}[\mathrm{SST} - T(z=h)]}_{\mathrm{C}} + \underbrace{\frac{(k\partial_z T)(z=h)}{h}}_{\mathrm{D}} \\ &\underbrace{+\frac{Q^* + Q_s[1 - f(z=h)]}{\rho_0 C_p h}}_{\mathrm{E}},\end{aligned} \tag{2}$$

where the angle brackets denote the vertical average over the mixed layer h (with our notation, h is positive). Here, $\langle x\rangle = (1/h)\int_0^h x\, dz$. In Eq. (2) term A is the advection, B is the lateral diffusion, C is the entrainment–detrainment at the mixed layer base, D is the vertical diffusion flux at the mixed layer base, and E is the heat flux storage in the mixed layer, where Q^* is the nonsolar heat flux.

The mixed layer depth is calculated as the depth where the vertical density is 0.05 kg m^{-3} higher than the surface density. This is different from the criterion of 0.01 used by Vialard and Delecluse (1998b) and Vialard et al. (2001, 2002, 2003). However, as was argued by De Boyer-Montégut et al. (2004), the criterion of 0.05 is more appropriate for equatorial regions. With a crite-

rion of 0.05 the model mixed layer depth compares better with the climatology of De Boyer-Montégut et al. (2004) (not shown). It was verified that choosing other criteria such as 0.01 or 0.03 kg m^{-3} gave virtually the same results. In the model, the term C for entrainment–detrainment is essentially negligible, as discussed in appendix A. This term will thus be neglected in further computations.

Each of the separate terms in Eq. (1) is computed by the ocean model and stored as a daily average. For Eqs. (1) and (2), it was verified that each term, except the vertical diffusion terms, could be recalculated with daily variables with an error of about 1% relative to what is found with the instantaneous outputs. In other words, the model T, u, v, and w variables do not exhibit much energy at frequency higher than 1 day (there is no diurnal cycle in the simulations considered in this paper) and so the correlation between terms on a daily average and the daily variations of the mixed layer can be neglected. We are aware of the diurnal cycle mixing in the upper equatorial Pacific Ocean induced by deep cycle turbulence (Lien et al. 1996), but addressing this issue is well beyond the scope of our present study.

Each variable X can then be separated offline into a low-frequency component (subscript m as "mean") and an eddy component (prime); for example,

$$X = X_m + X'. \tag{3}$$

Previous studies have shown that there is TIW-related variability in two distinct spectral bands. The first one is found at the equator with a period of about 20 days (Halpern et al. 1988; Lyman et al. 2005). This variability is distinct from that north of the equator (McPhaden 1996; Kennan and Flament 2000; Lyman et al. 2005) with a period near 30 days. The model configuration we use reproduces the two spectral peaks (Vialard et al. 2003), with around the 30-day period, a broad band of energy in the 20–50-day period. Ideally, filtering could separate the two 20-day and 30-day phenomena, but this is beyond the scope of the paper. We will here consider both time scales of variability together and refer to them collectively as "eddy variability" or TIWs. As TIWs in the model have a broad spectral peak in the 20–50-day range (Vialard et al. 2003), we use a 70-day boxcar filter to separate the "low-frequency part" from the eddy part. Thus, the eddy part in fact contains most of the energy at periods lower than 60 days. This encompasses not only TIWs but also a small portion of the intraseasonal Kelvin waves. Nevertheless, it was confirmed that TIWs stand out as the dominant signal in the eastern Pacific.

Based on this decomposition, each of the advective terms can be decomposed into four terms: for example,

$$-u\partial_x T = -u_m\partial_x T_m - u_m\partial_x T' - u'\partial_x T_m - u'\partial_x T'. \tag{4}$$

To evaluate the effect of TIWs on the heat budget on seasonal time scales, Eq. (1) can then be averaged over a long period (denoted by an overbar). If this period is sufficiently long, which is the case here (since we will consider the entire 1993–96 period), the storage terms $\partial_t T$ becomes negligible and we are left with the following balance for the temperature Eq. (1):

$$\underbrace{-\overline{u_m\partial_x T_m - v_m\partial_y T_m - w_m\partial_z T_m}}_{\text{A}} \underbrace{-\overline{u'\partial_x T' - v'\partial_y T' - w'\partial_z T'}}_{\text{B}} + \underbrace{\overline{D_z(T) + D_l(T) + I(z)}}_{\text{C}} \approx 0. \tag{5}$$

We checked that cross mean-eddy terms such as $\overline{u'\partial_x T_m}$ were indeed vanishing in the long-term budget. In Eq. (5), term A represents the climatological effect of advection and B denotes the advection due to the eddies. Term C will be named diabatic effects. The vertical diffusion term $D_z(T)$ also exhibits a clear signal on TIW scales. This term can be separated into a mean and an eddy component, but with an error of ~15%. It has to be treated differently than the advection terms (see appendix B for details).

The time-averaged equation for SST can be written as

$$\underbrace{\overline{\langle -u_m\partial_x T_m - v_m\partial_y T_m - w_m\partial_z T_m\rangle}}_{\text{A}} + \underbrace{\overline{\frac{1}{h}(k_m\partial_z T_m)_{z=h}}}_{\text{B}} + \underbrace{\overline{\langle -u'\partial_x T' - v'\partial_y T' - w'\partial_z T'\rangle}}_{\text{C}} + \underbrace{\overline{\frac{1}{h}(k\partial_z T - k_m\partial_z T_m)_{z=h}}}_{\text{D}} + \underbrace{\overline{\langle D_l(T)\rangle}}_{\text{E}} + \underbrace{\overline{\left\langle \frac{Q^* + Q_s(1 - f(z=h))}{\rho_0 C_p h}\right\rangle}}_{\text{F}} \approx 0. \tag{6}$$

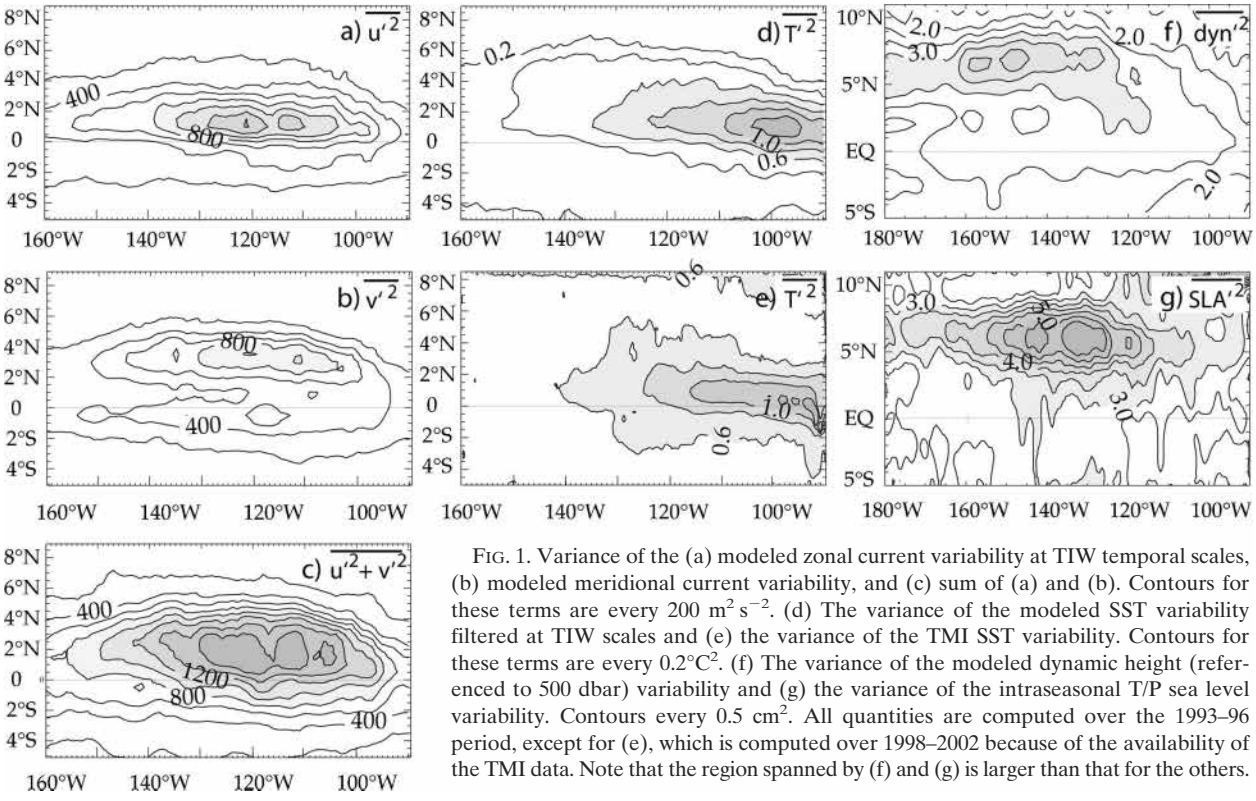

FIG. 1. Variance of the (a) modeled zonal current variability at TIW temporal scales, (b) modeled meridional current variability, and (c) sum of (a) and (b). Contours for these terms are every 200 $m^2 s^{-2}$. (d) The variance of the modeled SST variability filtered at TIW scales and (e) the variance of the TMI SST variability. Contours for these terms are every $0.2°C^2$. (f) The variance of the modeled dynamic height (referenced to 500 dbar) variability and (g) the variance of the intraseasonal T/P sea level variability. Contours every 0.5 cm^2. All quantities are computed over the 1993–96 period, except for (e), which is computed over 1998–2002 because of the availability of the TMI data. Note that the region spanned by (f) and (g) is larger than that for the others.

In Eq. (6), term A stands for the advection by mean currents, B is for the mean effect of vertical diffusion flux at the mixed layer base, C is for the TIW-induced advection, and D is for the TIW-induced diffusive vertical heat flux at the mixed layer base. In addition, term E is a parameterization of lateral heat diffusion processes by small-scale processes and can be thought as part of the eddy contributions. Term F represents the effect of air–sea heat fluxes on SST.

3. The simulated tropical instability waves

In this section, we will show some validations of the TIW statistical properties and three-dimensional circulation patterns. Figure 1b shows that the meridional eddy velocity variance in the 160°–90°W region is in quite good agreement with estimates derived from drifter observations (Baturin and Niiler 1997, their Plate 4c). Consistent with the observations, the model reveals a double-peak pattern. One peak is located along the equator near 120°W, with values reaching 600 $cm^2 s^{-2}$, while the second is to the north between 100° and 140°W with peak values near 1000 $cm^2 s^{-2}$. These values are approximately 25% lower than those of Baturin and Niiler (1997). The zonal eddy velocity variance is more homogeneous with one maximum area with values reaching 1200 $cm^2 s^{-2}$ at 1°N, 110°W (Fig. 1a). Overall, the patterns seen here for the horizontal eddy velocity variances are similar to the ones given in the modeling study of Harrison et al. (2001, their Fig. 11).

The pattern of modeled eddy temperature variance shown in Fig. 1d is comparable to a similar quantity from the 1999–2003 Tropical Rainfall Measuring Mission (TRMM) Microwave Imager (TMI) observations (information online at http://www.remss.com/) filtered at the same frequencies. The main variability region, consistent with the findings of Chelton et al. (2001), is seen to be located near 1°N with observed values reaching $1.2°C^2$ near 100°–90°W for both observations and the model. While the spatial pattern is similar in the model and in the observations, the modeled SST variability underestimates that found in the observations by about 20% in the region 2°S–6°N, 100°–160°W. The modeled dynamic height eddy anomalies (referenced to 500 dbar) are compared with the Ocean Topography Experiment (TOPEX)/Poseidon (T/P) ERS (Aviso) dataset. Again, while the spatial patterns are comparable to observations with a peak of dynamic height variability near 6°–7°N, from 120° to 160°W, the model underestimates sea level variability by about 30%.

Overall, the comparisons show that the patterns of modeled eddy variability are consistent with observa-

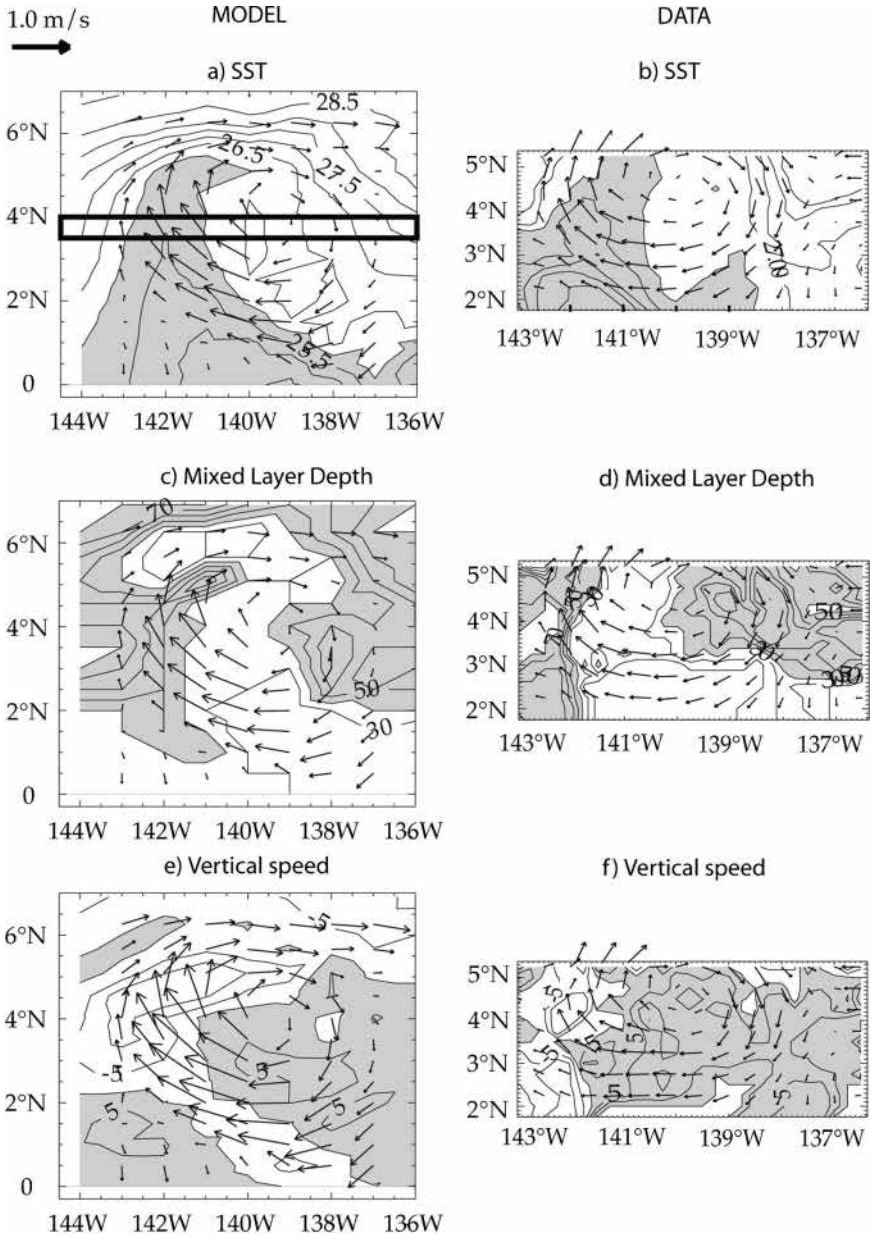

FIG. 2. Comparison of (a), (c), (e) model snapshots and (b), (d), (f) the results of Kennan and Flament (2000). For the model, snapshots are taken on 12 Oct 1996. In (a) SST is contoured every 0.5°C and shaded below 26°C for clarity with mixed layer currents minus -0.45 m s^{-1}, the mean westward wave speed (see Fig. 4 and text). In (b), SST is contoured every 0.25°C and shaded below 26.75°C for clarity. In (c), (d) the mixed layer depth is contoured every 10 m with shading above 40 m for clarity. In (e), (f) the vertical speed anomalies at the mixed layer depth are contoured every 5 m day^{-1} with zonal current anomalies averaged over the mixed layer. Positive values of the vertical speed (upwelling) are shaded. The box in (a) represents the area for the vertical section shown in Fig. 3.

tions even though the variances of eddy current, eddy temperature, and eddy sea level height are about 25% too weak. The typical amplitude of TIWs in the model (square root of the variance) is thus underestimated by roughly 15%.

Having considered a large-scale validation of surface fields, we will now turn our attention to validation of the three-dimensional patterns within TIWs. Figure 2 shows a visual comparison between the model TIWs and observations from Kennan and Flament (2000).

Figure 2a shows the typical structure of the SST and the current associated. The same is shown for the data in Fig. 2b. Cold water cusps are associated with northwestward velocities in the leading edge of the eddies while warm waters are seen in the trailing edge with the returning flow. Tangential speeds reach 1 m s^{-1}, consistent with observations. Downwelling (Figs. 2e and 2f) is found in the leading edge of vortices with values reaching ~5–10 m day^{-1} at the mixed layer base, and upwelling is seen in the vortex center with coherently similar values (remarkably enough) in both the model (Fig. 2e) in the observations (Fig. 2f). These patterns are depicted in other numerical simulations (e.g., Philander et al. 1985; Harrison 1996). The good agreement with observations of the vertical speed at the mixed layer bottom suggests that we can indeed use the model to estimate the effect of TIWs on the SST heat budget, as targeted in this study. At the TIW scale, the mixed layer depth varies widely, with values of ~10–30 m in the cold water region, increasing to 50–100 m to the north in the strongest downwelling region and in the eastern side of the vortex in both data and observations (Figs. 2c and 2d). Unexpectedly, in the upwelling region of the trailing edge of the vortex, the mixed layer also deepens locally in both the data and observations.

Overall, the amplitude of these mixed layer variations serves to emphasize the fact that constant depth budget studies may not be appropriate in helping to understand the SST variability at TIW scales. The horizontal SST and current structure also suggest a strong influence of horizontal advection in the SST budget (e.g., northward currents seem to transport cold equatorial water to the north in the leading edge of the vortex). On the other hand, the vertical movements seem at odds with the mixed layer and SST variations in the vortex center where warm waters and a deeper mixed layer are found in the upwelling region. This already suggests a comparatively smaller influence of vertical advection on the SST.

The TIWs shown in Fig. 2 are found to propagate in the model at about -0.45 m s^{-1} (see Fig. 4 and discussion in the beginning of section 4). To facilitate comparison with observational analyses (i.e., Kennan and Flament 2000), a vertical section is performed through the vortex center, see Fig. 3, as depicted by a box in Fig. 2. This section is comparable to that shown in Fig. 23 of Kennan and Flament (2000). Although the observed and modeled vortices correspond to different times and locations, they show a remarkably similar structure. First, the horizontal currents associated with the TIW are mostly confined from the surface to the upper thermocline (Figs. 3a and 3e). In both the data and observations, the strongest northward flow surfaces while the southward returning flow has a maximum between 50 and 100 m. This tilted structure is coherent with a circulation pathway whereby the surface equatorial waters downwell at the leading edge and return at depth in the trailing edge of the vortex as was found by Kennan and Flament (2000) and Menkes et al. (2002). Both modeled and observed temperature structures are qualitatively similar. They have a complex structure with a deepening of the thermocline and halocline cores at the vortex center, with this deepening being out of phase with changes in mixed layer depth, as the mixed layer depth is thinnest at the vortex center near the upwelling region (see also Figs. 2e and 2f). This again indicates a decoupling between the thermocline depth and the mixed layer depth. Last, in the leading edge of the vortex, the surface downwelling is tightly associated with the SST front (Figs. 3b–e). Associated with the upwelling and downwelling movements in Fig. 3e, there is a surface layer convergence on the western side of the vortex and a surface divergence (upwelling) close to its center with similar amplitudes both in the model (Fig. 3d) and observations. The major difference between the model and data is that TIW-induced vertical currents in the thermocline are underestimated by roughly a factor of 2 by the model (~50 versus ~25 m day^{-1}). However, it should be pointed out that, first, the vertical currents have correct amplitude at the mixed layer bottom, and second, the errors in the observations are magnified with depth. Thus, it is reasonable to estimate the effects of TIW vertical advection on the SST budget over the mixed layer. Below the mixed layer, the estimates of $\overline{-w'\partial_z T'}$ may conservatively be viewed as lower limits. This will be discussed further in section 6b.

4. Heat budget at the spatial and temporal scale of tropical instability vortices

We now turn to the model simulation to investigate the heat budget at the scales of TIW variability. This analysis is based on the decomposition of the SST equation described by Eq. (2) where all terms are decomposed in mean and eddy terms [see Eqs. (3) and (4)]. To describe the robust features associated with TIWs in the heat equation, we constructed a composite as follows. In October 1996, instabilities are fully developed west of 100°W with vortices propagating westward with relatively constant speed during 1 month as can be seen in Fig. 4. Starting on 1 October 1996, we average daily snapshots (such as those presented in Fig. 2) in a box translated at that constant speed (Flament et al. 1996), in order to follow a train of waves as it propagates westward. If the tropical instability vortices (TIVs) were steady in the propagating frame, the rate of SST

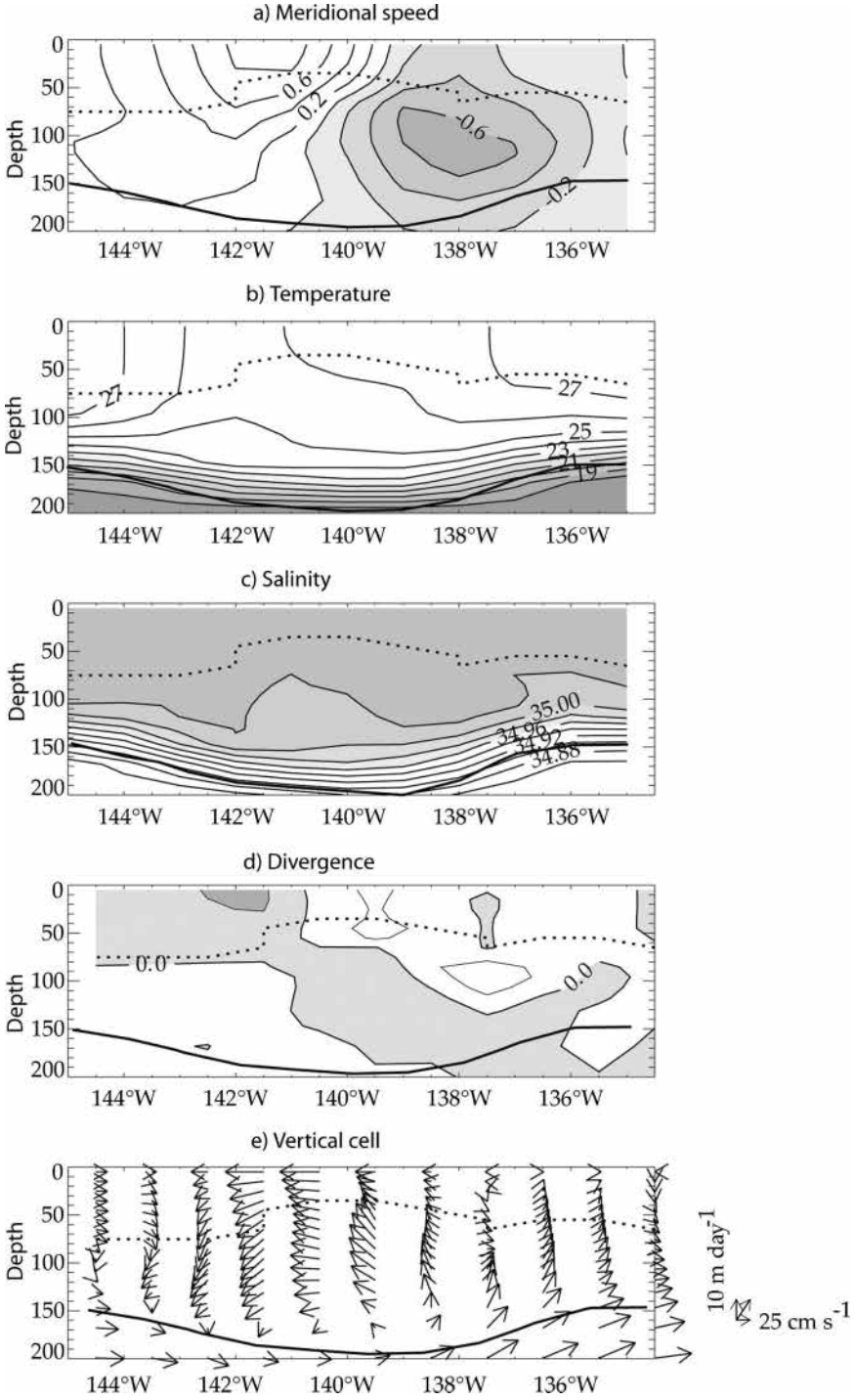

FIG. 3. A section similar to that of Fig. 23 in Kennan and Flament (2000). Vertical section averaged between 3.5° and 4°N, as depicted in Fig. 2a, on 12 Oct 1996 of (a) meridional currents. Negative currents are shaded and contours are every 0.2 m s^{-1}. The depth of the pycnocline (σ_θ = 24.7 kg m^{-3}) is indicated as a solid line and the mixed layer depth is dotted. (b) Same as in (a), but for temperature. Contours are every 0.5°. (c) Same as in (a) but for salinity. (d) Same as in (a), but for current divergence scaled by 1×10^{-6} for clarity. Contours are every 0.5 s^{-1}. Convergence is shaded. (e) Same as in (a), but for velocity arrows. Note that the scales for the horizontal and vertical velocities are different.

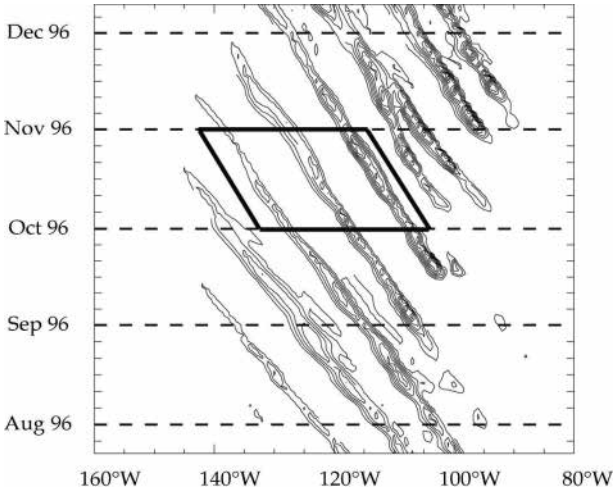

FIG. 4. Longitude time section of the SST in the 1°–2°N band, contoured every 0.5°C. For clarity, only contours for SST below 26°C are plotted. The slanted box indicates the area where the composite of Fig. 5 is constructed following the TIW propagation (at $c = -0.45$ m s^{-1}). The box contains three TIWs.

change in this frame would be zero. The mean westward translation speed was adjusted so as to minimize this rate [as in Kennan and Flament (2000) and Menkes et al. (2002)]. The resulting speed of about $c = -0.45$ m s^{-1} is displayed in Fig. 4 by the slanted box. Figure 5 thus represents the typical SST budget in a frame of reference that moves with the TIW disturbance. Only the terms that contribute significantly to the heat budget have been plotted in these figures.

In the moving frame, the storage term (Fig. 5b) is small compared to the other terms. This shows that the heat budget following the vortices is to first order steady, as hypothesized. Zonal advection (Fig. 5c) is dominated by the eddy nonlinear advection term $-u'\partial_x T'$, which heats the SST equatorward of 4°N (Fig. 5d) in the cold cusps, and by the effect of $-(u_m - c)\partial_x T'$ (Fig. 5e). The sign of this term illustrates the fact that, even in the moving frame, the current is faster than the wave and thus tends to distort the cusp shape by cooling the leading edge and heating the trailing edge of the waves south of 4°N. It is the balance with the other terms that allows the TIW to preserve its shape when propagating. The two terms that contribute significantly to meridional advection are $-v'\partial_y T_m$ (Fig. 5h) and $-v'\partial_y T'$ (Fig. 5g). The term $-v'\partial_y T_m$ has negative contributions on the leading edge of the eddy (where the current is northward) and positive ones on the trailing edge (were the current is southward) and is in phase with the temperature signal. That term thus acts to maintain the north–south SST structure. The total advection pattern (Fig. 5i) is dominated by horizontal eddy advection (Fig. 5j), which acts primarily to heat the cold cusp and to a lesser extent warm the warmest areas. As suggested before, vertical advection does not contribute significantly to the mixed layer heat budget at this scale and is thus not shown. This is the result of a combination of weak vertical velocities and weak vertical gradients at the mixed layer bottom that make that term comparatively smaller than the horizontal advection.

Since the nonlinear terms $-u'\partial_x T' - v'\partial_y T'$ are the relevant ones when considering the long-term TIW contribution to the SST budget [terms like $-(u_m - c)\partial_x T'$ or $-v'\partial_y T_m$ vanish in the long-term average], they merit more detailed consideration. A schematic is presented in Fig. 6 that facilitates identification of the spatial patterns of u', v', and T', which will be referred to in the discussion that follows. Figure 6a shows again the temperature and currents associated with the composite in Fig. 5a. Figure 6b shows the mixed layer temperature and horizontal current anomalies (u', v', and T'). Between the anticyclonic eddies, cyclonic anomalous currents can be seen. These eddies are asymmetric: the westward flow south of 4°N is stronger and wider than the eastward flow between 5° and 6°N (Figs. 2a–c) These cyclonic and anticyclonic currents converge into a northward (southward) flow region collocated with a negative (positive) temperature anomaly, resulting from the northward (southward) displacement of the north equatorial front (Fig. 6b).

The cyclonic and anticyclonic eddies show a broader and stronger zonal flow in the 0°–4°N band, as noted above. Thus, eddy zonal advection is stronger in that band (Fig. 5d). The $-u'\partial_x T'$ term is always associated with a warming (Fig. 5d), because westward eddy currents are located in a region of positive $\partial_x T'$ (region A in the idealized sketch Fig. 6c) and eastward eddy currents in a region of negative $\partial_x T'$ (region B). The term $-v'\partial_y T'$ is associated with warming between 2°S and 2°N, patches of cooling between 2° and 4°N, and patches of warming between 4° and 6°N. It can be explained as follows (see sketch in Fig. 6d). The temperature anomaly displays two maxima, one located around 1°–2°N, corresponding to north–south excursion of the temperature front, and one around 4°–5°N. As seen in the sketch, the northward flow is collocated with negative temperature anomaly regions. This results in a positive $-v'\partial_y T'$ in the region denoted A in the sketch, negative value in region B and, positive value again in region C. In regions where the flow is southward, the temperature anomalies are positive, resulting in the same pattern.

The remaining dominant term in Fig. 5 is the vertical diffusion (Fig. 5l) separated into mean (Fig. 5m) and

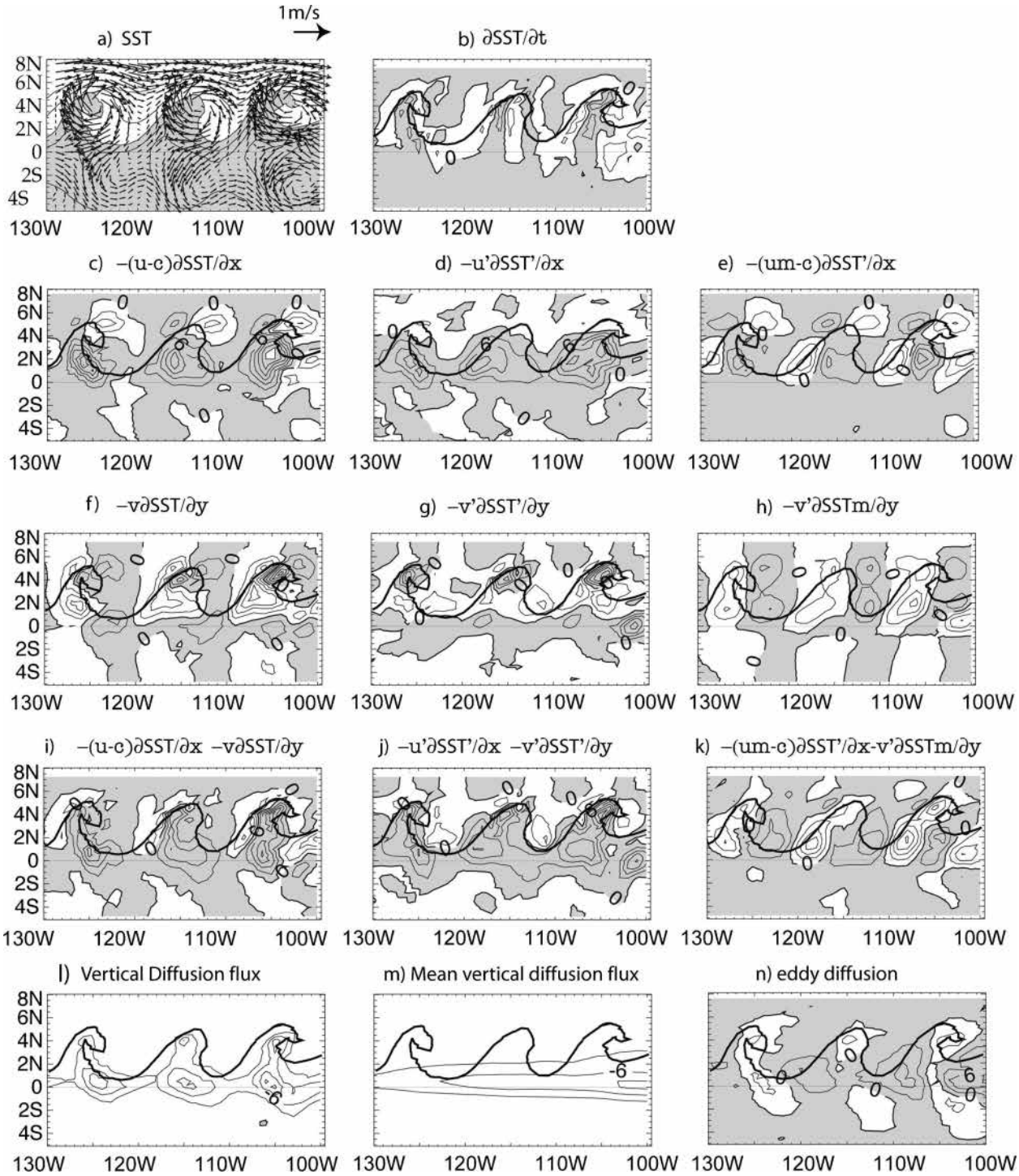

FIG. 5. Composite of the various terms of the mixed layer heat budget, constructed by averaging the quantities in the westward-moving translating frame in Fig. 4. The temperature trends correspond to the terms described in Eq. (2). (a) Temperature and currents. The remaining panels represent the dominant terms of the SST trends (°C month^{-1}) except for (b) where TIWs are almost steady in SST in the translating frame: (b) $\partial_t T$, (c) $-(u - c)\partial_x T$ [sum of (d), (e)], (d) $-u'\partial_x T'$, (e) $-(u_m - c)\partial_x T'$, (f) $-v\partial_y T$ [sum of (g), (h)], (g) $-v'\partial_y T'$, (h) $-v'\partial_y T_m$, (i) $-u\partial_x T - v\partial_y T$ [sum of (c), (f)], (j) $-u'\partial_x T' - v'\partial_y T'$ [sum of (d), (g)], (k) $-(u_m - c)\partial_x T' - v'\partial_y T_m$ [sum of (e), (h)], (l) $(1/h)(k\partial_z T)_{z=h}$ [sum of (m), (n)], (m) mean vertical eddy diffusion $(1/h)(k_m\partial_z T_m)_{z=h}$, and (n) eddy contribution to vertical eddy diffusion $(1/h)(k\partial_z T - k_m\partial_z T_m)_{z=h}$. Positive values are shaded and contours are every 3°C month^{-1}; the 26°C isotherm contour was added in each panel to facilitate locating the TIW structure.

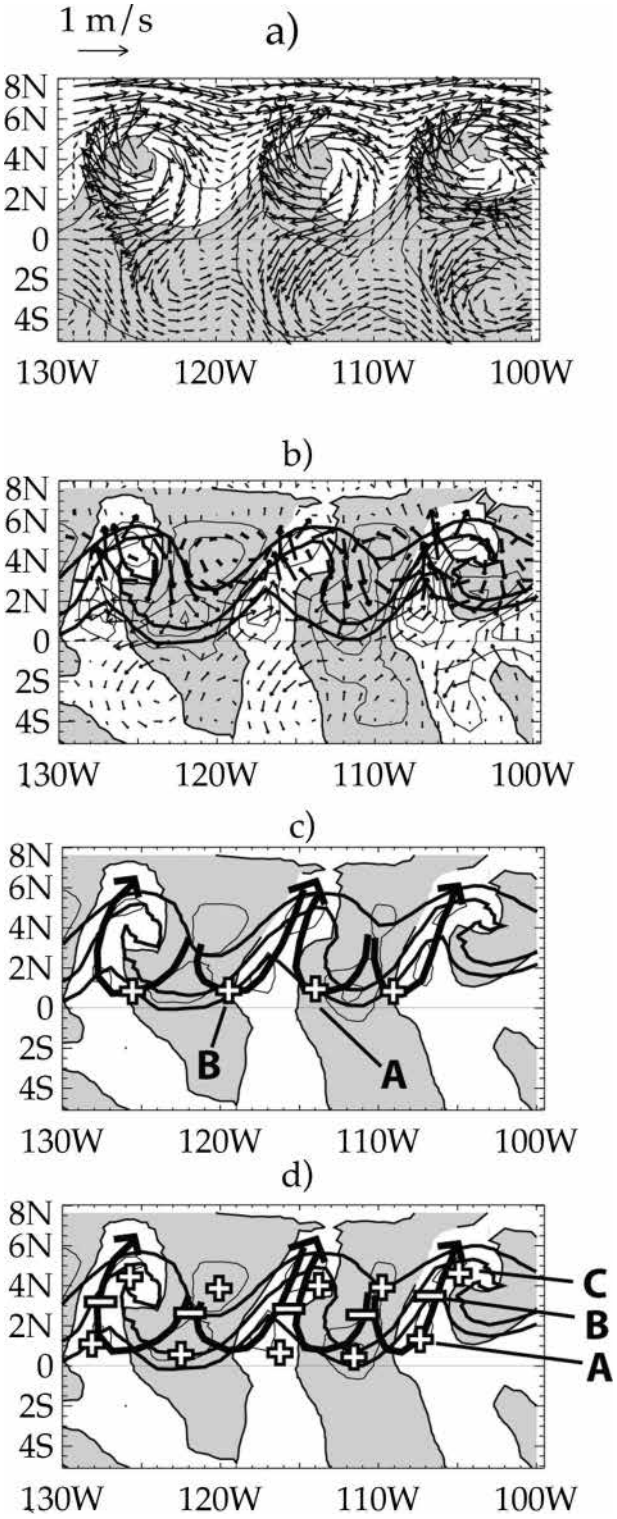

FIG. 6. Sketch summarizing the processes associated with horizontal eddy advection $-u'\partial_x T' - v'\partial_y T'$. (a) Same as in Fig. 5a. (b) TIW mixed layer currents u', v' (vectors) and temperature anomalies T' (contours). (c) Sketch explaining how correlations between T' and u' result in $-u'\partial_x T'$ patches. (d) Same as in (c) but for $-v'\partial_y T'$ patches. In (c), (d), the plus (+) and minus (−) signs indicate the sign of the corresponding zonal and meridional advections, respectively.

eddy (Fig. 5n) contributions. There clearly is a modulation of the vertical diffusion flux by the TIWs as seen in Fig. 5l. Vertical diffusion cools actively in regions of cool temperature mimicking the cusplike shape of SST while it is weaker in the warmer temperature areas. The reason for this modulation is mainly due to variations in the vertical eddy diffusivity $(k)_{z=h}$ at the TIW scales with enhanced diffusivity in the coldest region of the cold cusp where the mixed layer is thin and the stratification shallow (Figs. 2b and 3b). There, $(k)_{z=h}$ is strong at the mixed layer base. Similarly, diffusivity is reduced in the trailing edge of the TIW in warm areas where the mixed layer is deeper (Fig. 2b). The effect of TIWs is thus mostly to enhance cooling via vertical diffusion in the cold cusps and to reduce it in the warm areas (Fig. 5n).

The mixed layer budget is thus dominated by horizontal advection heating the cold tongue and cooling to the north of the equatorial front, with no significant contribution from vertical advection. It has to be noted, however (though not shown), that the TIW-induced vertical advection becomes significant below the mixed layer and has to be considered when looking at a heat budget including the thermocline. This could be expected, since Fig. 3 shows stronger TIW vertical speeds and temperature gradients below the mixed layer. The consequences of this on the long-term heat budget of the cold tongue will be discussed in the following sections.

5. Impact of TIWs on the climatological heat budget of the cold tongue

In this section, we will investigate how TIWs contribute to the long-term heat balance in the cold tongue. We will first look at the vertical structure of the heat budget. We will then quantify the overall effect of TIWs on the SST balance.

a. Vertical structure of the heat budget

Figure 7 represents the zonal average over 160°–90°W (which was revealed in Fig. 1 to be the region of highest TIW activity) of the terms in Eq. (5), as a function of latitude and depth. The figure is organized such that the first three panels of the first column show the total zonal, meridional, and vertical advection terms of the equation. The second column of the three first rows represents the mean advection terms of Eq. (5), and the last column of the three first rows the eddy terms. Figure 7j shows term C of Eq. (5). Figure 7k shows term A of Eq. (5) (total mean advection), and Fig. 7l shows the total eddy advection. [term B of Eq. (5)].

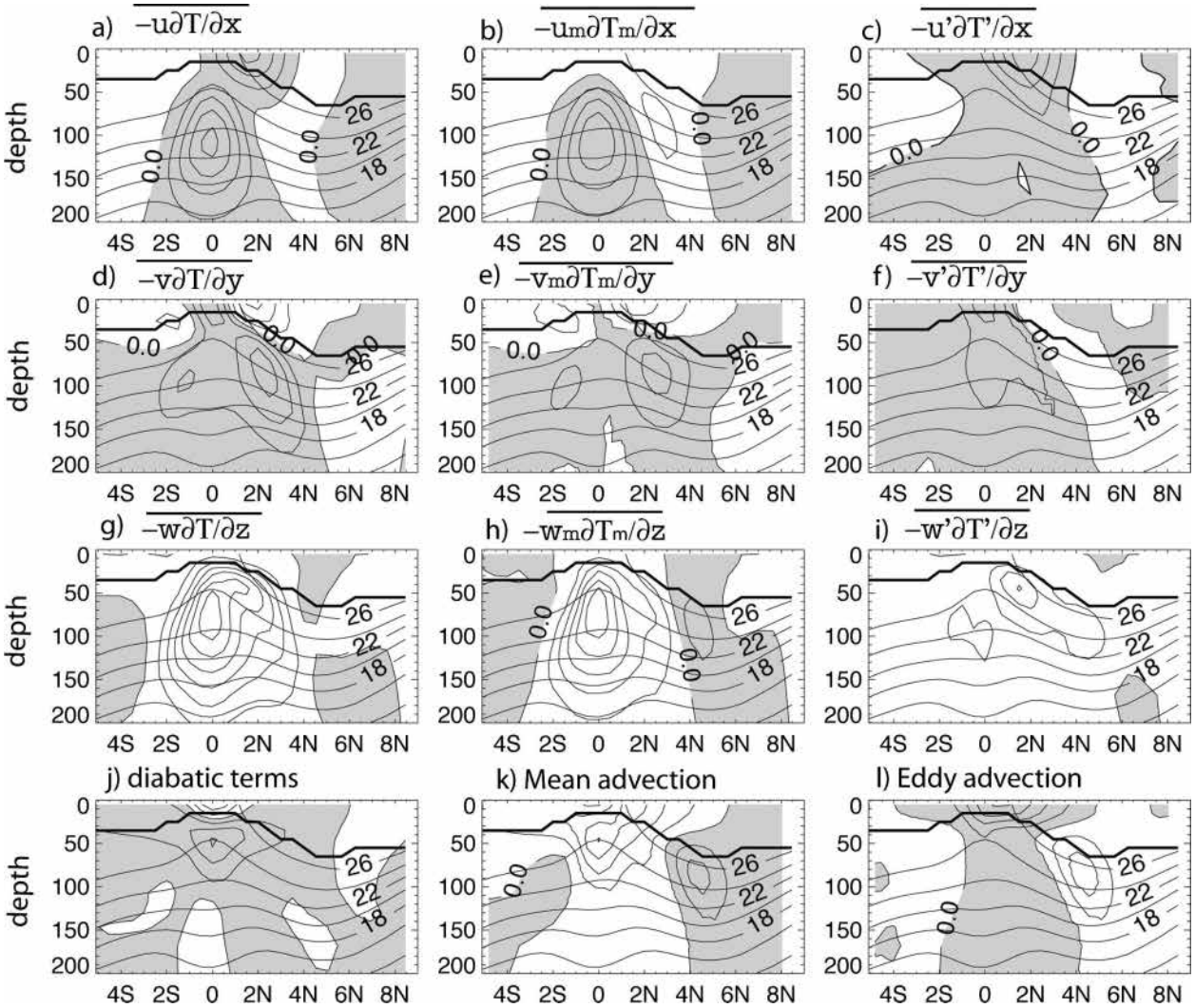

FIG. 7. Shaded and contoured, the mean vertical section of temperature trends averaged over 1993–96 for the 160°–90°W box corresponding to the balance described in Eq. (5). Gray shades indicate positive values (warming) and contours are every 0.5°C month^{-1}. The mean mixed layer depth for the same period is indicated as a thick line. Temperature contours (every 2°C) are superimposed. Terms (a) $-\overline{u\partial_x T}$, (b) $-\overline{u_m\partial_x T_m}$, and (c) $-\overline{u'\partial_x T'}$. (d)–(f) Same as in (a)–(c) but for meridional advection. (g)–(i) Same as in (a)–(c) but for vertical advection. (j) Diabatic terms (vertical diffusion + surface heat fluxes), (k) mean advection terms, and (l) eddy advection terms.

Below the mixed layer, zonal advection (Fig. 7a) is dominated by warming due to mean currents: the Equatorial Undercurrent (EUC) carries warm water eastward, with tendency values reaching 2°C month^{-1} in the EUC core (Fig. 7b). In the mixed layer, zonal advection is dominated by TIW warming, which is strongest between the equator and 4°N, and reaching 2°C month^{-1} (Fig. 7c). Such mean TIW-induced zonal advection could be inferred by the patterns described in Fig. 5 where a strong warming pattern is seen at TIW scales near 2°N (see section 4 and Fig. 5d).

The mean meridional advection reflects the effect of the equatorial cell, with divergence at the surface, exporting cool water from the cold tongue, and equatorward flow below, bringing in warm water (Fig. 7e). Mean meridional advection is strongest in the Northern Hemisphere where meridional temperature gradients are strongest. The TIW-induced meridional advection is mainly concentrated between 1°N and 1°S, with warming reaching 1°C month^{-1} in the mixed layer (Fig. 7f) but with significant warming down into the thermocline. The mean warming close to the equator is coherent with the composite in Fig. 5g and the sketch in Fig. 6d. However, the patterns of strong local eddy cooling and warming centered at 2° and 4°N in Fig. 5g fade out in the mean, because of the spreading of the

meridional distribution of the instantaneous patterns and, for the pattern at 4°N, to the alternating positive and negative areas.

Vertical advection is responsible for 3°C month^{-1} of cooling in the upper part of the EUC (Fig. 7g) and is largely dominated by the mean equatorial upwelling (Fig. 7h). Mean vertical advection is associated with a strong cooling in the equatorial upwelling (up to 2.5°C month^{-1}) and moderate warming (0.5°C month^{-1}) in the downwelling region around 5°N.

Of primary interest to this study is the TIW contribution in the vertical advection. It was our intention to identify whether it counteracts TIW-associated horizontal advection as suggested in V01 and Jochum et al. (2004) and, if so, to what extent. The mean TIW-induced vertical advection (Fig. 7i) has mainly a cooling effect (up to 1.5°C month^{-1}) and is strongest below the base of the mixed layer (between 30 and 100 m), between 2°S and 5°N, where horizontal TIW-induced advection is a warming contribution. The total integrated TIW-induced advection (Fig. 7l) shows that horizontal effects offset the vertical. Yet, in the mixed layer the TIW-induced vertical advection is small. TIWs thus contribute to warm the mixed layer by up to 2°C month^{-1} between 2°S and 4°N. Within 2°S–2°N, below the mixed layer, both horizontal and vertical effects almost compensate, resulting in a weak warming. Farther north (3°–5°N) the overall effect of eddies is to cool by up to 1°C month^{-1} between 50 and 130 m. Overall TIW-induced advection tends to diminish the temperature gradient between the cold tongue and the warm water pool lying north of it.

Figures 7j–l show a summary of the heat balance over 1993–96. Overall, there is a balance between mean and TIW-induced advection, except at the equator, where the strong surface forcing is redistributed vertically within the ocean by vertical mixing (cooling the surface and warming the subsurface). This overall heat balance is thus the result of a complex interplay between the mean and eddy advection, and the factors controlling the mixed layer temperature (SST) are seemingly different from those controlling the temperature beneath.

b. Mixed layer heat budget: The SST balance

It was noted above that the TIW contributions were radically different in the mixed layer and below. The mean mixed layer heat balance (relevant to SST) is now examined more closely. Figure 8 shows the 1993–96 average of the mixed layer temperature equation, as presented in Eq. (6). It is also the time average of snapshots such as that presented in Fig. 5. As could be expected from the previous discussions, the contribution of TIW-induced vertical advection to the SST budget is negligible (Fig. 8g) and TIW-induced horizontal advection is a heating contribution to the SST balance in the cold tongue (up to 3°C month^{-1}). Lower-frequency advection (Fig. 8d) acts to counteract this effect by cooling mainly via meridional and vertical advection (Figs. 8b,c) in the same latitudinal band, but the overall budget for total advection is still a heating near the equator (Fig. 8l) due to TIWs.

In addition, the mean contribution of TIW-induced vertical mixing is also a warming, centered at the equator (Fig. 8n) with a heating equivalent to horizontal TIW advection just near the equator. While the mean heating patterns from TIW horizontal advection can be easily understood from Figs. 5 and 7 and their discussions, a closer look at Fig. 5n is needed to understand the mean heating by TIW vertical mixing. In Fig. 5n, the areas of warming have larger spatial extensions than the cooling areas, especially near the equator, because the cold crests have smaller spatial extensions than the warmer areas between. Thus, when waves are passing by, the net effect is a cancellation of the cooling area and a global heating near the equator as seen in Fig. 8n. As discussed in appendix B, the error on that term is about 15%. Thus, the model suggests that all the terms associated with TIWs contribute to warm the SST in the cold tongue from 2°S to 4°N. Last, the SST budget is closed by the additional heating by the atmospheric fluxes trapped in the mixed layer (Fig. 8k) and the cooling provided by the low-frequency vertical heat diffusion at the mixed layer base.

6. Summary and conclusions

a. Summary

In this study we have used a numerical experiment with the LODYC ocean general circulation model to investigate the three-dimensional contribution of tropical instability waves to the tropical Pacific heat budget. Model validation reveals that the model has realistic spatial patterns in terms of surface eddy velocity variances, surface temperature, and sea level variance, but variances may be underestimated by up to 25% (i.e., TIW-associated signals are about 15% too weak in the model). Validation of the model results against observational data (Kennan and Flament 2000) shows that TIWs in the model have a qualitatively correct three-dimensional circulation and thermal structure. The main shortcoming of the model is that vertical speeds associated with TIWs are smaller (of the order of 25 m day^{-1}) than those deduced from Kennan and Flament (2000)'s observations (on the order of 50 m day^{-1}) in the upper thermocline. This may be due to the coarse-resolution model used here ($\sim$1°) relative to the obser-

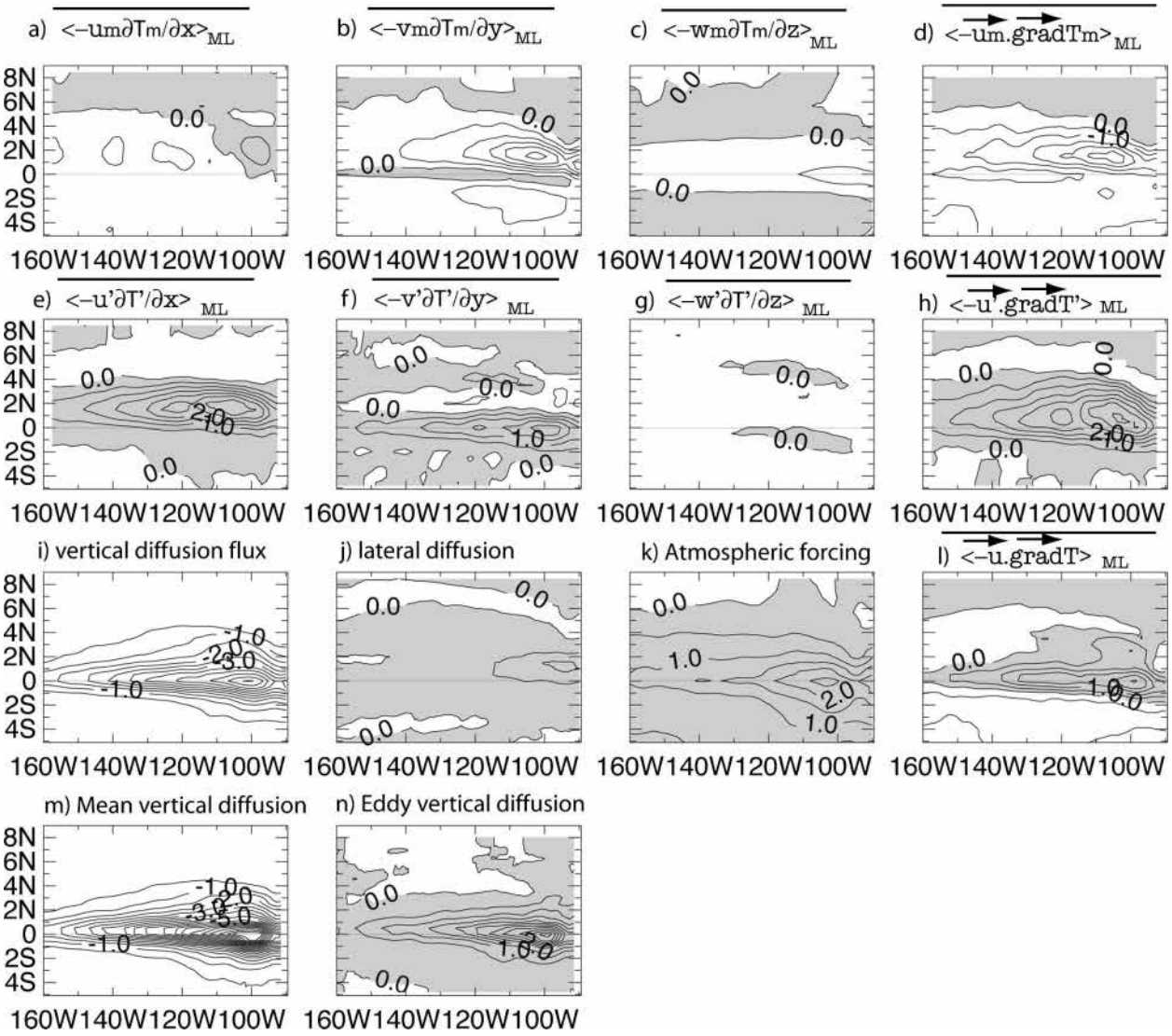

FIG. 8. SST budget over the 1993–96 period [cf. Eq. (6)]. Shading used for positive values. Contours are every 0.5°C month^{-1}. Terms (a) $\overline{-\langle u_m \partial_x T_m \rangle}$, (b) $\overline{-\langle v_m \partial_y T_m \rangle}$, (c) $\overline{-\langle w_m \partial_z T_m \rangle}$, (d) $\overline{\langle -u_m \partial_x T_m - v_m \partial_y T_m - w_m \partial_z T_m \rangle}$, (e) $\overline{-\langle u' \partial_x T' \rangle}$, (f) $\overline{-\langle v' \partial_y T' \rangle}$, (g) $\overline{-\langle w' \partial_z T' \rangle}$, (h) $\overline{\langle -u' \partial_x T' - v' \partial_y T' - w' \partial_z T' \rangle}$, (i) $\overline{(1/h)(k \partial_z T)_{z=h}}$, (j) lateral diffusion, (k) $\overline{\{Q^* + Q_s[1 - f(z = h)]\}/\rho_0 C_p h}$, (l) total advection [sum of (d), (h), (m) $\overline{(1/h)(k_m \partial_z T_m)_{z=h}}$ and (n) $\overline{(1/h)(k \partial_z T - k_m \partial_z T_m)_{z=h}}$. Brackets denote the average over the time-varying mixed layer; the overbar indicates the 1993–96 average.

vations (~0.25°) but also to uncertainties in the vertical speeds deduced from the observations. However, at the base of the mixed layer, the depth relevant for SST budgets, both model and data vertical speeds have similar spatial structures and amplitudes (of about 10 m day^{-1}). Thus, the representation of TIWs in the model is realistic enough to allow for an investigation of their impact on the surface layer heat budget (i.e., the SST equation balance). Nevertheless, future simulations should explore the TIW dynamics and heat balance at higher resolution.

As hypothesized in the data analyses of Flament et al. (1996), Kennan and Flament (2000), and Menkes et al. (2002), TIWs are relatively steady features, as they propagate, over a time scale of 1–2 months. In TIWs, the SST variability is controlled by a balance between horizontal advection, mainly a heating term, and vertical diffusion at the mixed layer base, a cooling term. Horizontal advection is dominated by $-u_m \partial_x T' - u' \partial_x T'$ where the second term, the eddy-induced horizontal advection, dominates and heats the 0°–4°N band and the first term helps the SST pattern to propagate westward. Meridional advection is on the order of zonal advection and is dominated by $-v' \partial_y T_m - v' \partial_y T'$, with

both terms acting equally in the SST budget at the TIW scale. It should be noted that $-v'\partial_y T_m$ is in phase with the temperature signal and acts to strengthen the eddy temperature structure but does not play a role in its propagation. Moreover, it averages to zero on seasonal and longer time scales. Vertical advection plays a negligible role in the SST anomalies of a typical TIW on all scales. This arises from the combination of weak vertical speeds acting on weak vertical gradients at the mixed layer base, relative to horizontal speeds and gradients. Below the mixed layer, however, TIW vertical advection cooling becomes more significant and induces a net cooling in the North Equatorial Countercurrent (NECC). Vertical advection is more significant in the upper part of the thermocline because it is where the major vertical gradients and vertical speeds are found. It is important to note that TIW heat balance is the result of a complex and sometimes subtle combination of almost all the vertical and horizontal processes.

The effect of TIW activity on the seasonal SST budget was investigated in the 160°–90°W band where TIWs are most active. The major patterns of cooling–warming are concentrated in the 2°S–6°N band and result from a delicate balance between TIW-induced horizontal advection, mean meridional advection, vertical diffusion, and atmospheric forcing. The SST balance is summarized in Table 1 for the 2°S–6°N, 160°–90°W band. Horizontal TIW advection heats by 0.84°C month^{-1} and low-frequency advection cools by –0.59°C month^{-1}, which allows total advection to warm the SST by 0.24°C month^{-1}. The remaining balance is ensured by atmospheric forcing that heats the mixed layer by 0.77°C month^{-1} and vertical diffusion that cools by −1.06°C month^{-1} (including an eddy-induced vertical diffusion heating of 0.37°C month^{-1}). Overall, the advective and diffusive processes associated with TIWs warm the area by 1.22°C month^{-1}, while the equivalent lower-frequency terms cool the SST by −2.02°C month^{-1}. TIWs are thus responsible for a first-order contribution to the SST budget in the cold tongue.

TABLE 1. The 2°S–6°N, 160°–90°W SST budget. TIWs are defined as phenomena that occur at scales on the order of a month or shorter. Low frequency is defined to have temporal scales greater than 1 month.

SST budget (°C month $^{-1}$)	Total	Low frequency	TIW
Zonal advection	0.38	−0.16	0.57
Meridional advection	−0.04	−0.30	0.27
Vertical advection	−0.11	−0.11	0.00
Total advection	0.24	−0.59	0.85
Vertical diffusion	−1.06	−1.43	0.37
Lateral diffusion	0.08		
Atmospheric forcing	0.77		

TIW-induced vertical advection thus plays a negligible role in the long-term SST balance. However, the three-dimensional long-term heat balance shows that this term becomes more significant below the mixed layer, as was the case for the heat budget at TIW scale.

Estimates of the eddy tendency in the model appear to be in the range of observations. For example, Bryden and Brady (1989) estimate an average heating by eddies of 1.6°C month^{-1} over the top 100 m between 100° and 150°W, along the equator. Our model gives 0.9°C month^{-1}, with 1.21°C month^{-1} warming from horizontal advection and 0.28 C month^{-1} cooling from vertical TIW advection. Swenson and Hansen's (1999) estimate is 0.7°C month^{-1} over the mixed layer for the 4°S–4°N, 100°–130°W box, while ours is 1.1°C month^{-1}, including 2% cooling from vertical TIW advection.

b. Discussion

In agreement with Vialard et al. (2001, 2003), we have shown that, consistent with what is found in observations, tropical instabilities heat the mixed layer in the eastern equatorial Pacific via horizontal heat advection—with both meridional and zonal advection being important. This also agrees with the model results of Vialard et al. (2001). Previous suggestions that there may be compensation between vertical cooling and horizontal warming associated with TIW activity were investigated. Our model experiments show that, as far as the SST is concerned, there is almost no compensation between TIW-induced horizontal advective warming and TIW-induced vertical advection cooling. On the other hand, McCreary and Yu (1992) and Pezzi and Richards (2003) showed that TIW amplitude and properties were sensitive to parameters like lateral mixing. Jochum et al. (2005) also showed that in a low-horizontal-resolution model of the Atlantic Ocean heating by TIWs can be dramatically reduced. This leads us to question whether the results are robust with respect to changes in parameterizations such as mixing or resolution. Indeed, improved mixing parameterizations for the cold tongue are currently at the forefront of climate modeling efforts.

The results we have shown here have differed from Vialard et al. (2001)'s only by the direction along which lateral diffusion is performed (our experiment is referred to as REF). In REF, this diffusion acts along isopycnals for both tracers and momentum-following recommendations of Lengaigne et al. (2003) and Pezzi and Richards (2003). However, to address the robustness of our results, we performed three additional sensitivity experiments: one with horizontal mixing (rather than isopycnal mixing) on both tracers and momentum

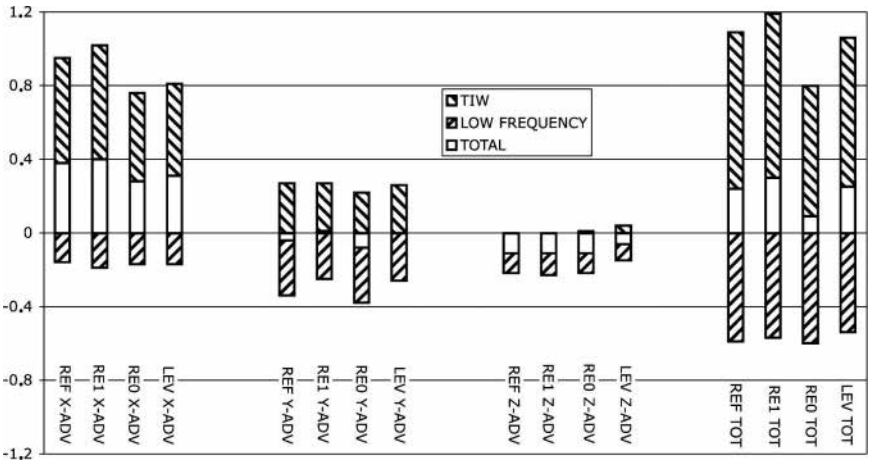

FIG. 9. Comparison between all of the advective terms (mean, eddies, and total currents) for the experiment used in this study (REF) that has isopycnal mixing on both tracers and momentum and three other sensitivity experiments: RE0, horizontal mixing on both tracer and momentum; RE1, isopycnal mixing on tracer and horizontal mixing on momentum; and LEV, similar as REF but with 10 times as many vertical levels (1-m resolution in the top 200 m). Advection units are in degrees Celsius per month. X-ADV stands for zonal advection, Y-ADV for meridional advection, Z-ADV for vertical advection, and TOT for the 3D advection.

[the experiment of Vialard et al. (2001) and (2003), referred to as RE0], one with isopycnal mixing on tracers and horizontal mixing on momentum (referred to as RE1), and a final one with isopycnal mixing on both momentum and tracers but with 10 times as much vertical resolution leading to 1-m resolution in the top 200 m (referred to as LEV). Figure 9 shows the results of the decomposition of the advective terms into the eddy and mean for the four experiments. The balance among the various terms is consistent across all of the experiments, with only slight differences. In particular, in none of the experiments does the TIW-induced vertical advection offset the horizontal TIW-induced advection. Thus, an important consequence of this study is that the consistent results of observationally based studies (Stevenson and Niiler 1983; Hansen and Paul 1984; Bryden and Brady 1989; Baturin and Niiler 1997; Swenson and Hansen 1999; Wang and McPhaden 1999; Kennan and Flament 2000) may not be overestimating the overall warming effect of TIW-induced advection on the SST of the cold tongue.

Our method was also applied in a similar study for the tropical Atlantic (Peter et al. 2006) in a higher-resolution Océan Parallélisé (OPA) model "CLIPPER" [⅙° lat × ⅙° lon; Tréguier et al. (2003)] and the results on the role of the TIWs on the tropical Atlantic seasonal SST budget are identical with almost no effects from vertical cooling due to TIWs in the SST budget. This is at odds with the results of the modeling study presented by Jochum et al. (2004) for the equatorial Atlantic. We would like to emphasize, however, that Jochum et al. (2004) based their results on heat flux divergences in a layer of 20-m depth taken as the mixed layer. For an SST budget, this may lead to biases as the mixed layer depth varies widely at TIW scales from 10 to 60 m. In addition, contrary to Jochum et al. (2004)'s method, we evaluated advective terms rather than flux divergences. Flux divergences involve small differences between large numbers and do not allow for separating out the influences of mass convergence. For an incompressible fluid the nonlinear terms may be written equivalently as the sum of advection or flux terms:

$$-u\partial_x T - v\partial_y T - w\partial_z T = -\partial_x(uT) - \partial_y(vT) - \partial_z(wT).$$

Consider a thermally homogeneous 2D ocean in motion. At any ocean point, the temperature evolution $\partial_t T$ is zero and advection (e.g., $-u\partial_x T$) is zero because there is no temperature gradient. However, $\partial_x(uT) = T\partial_x u$ (since $u\partial_x T = 0$) is not necessarily zero since u varies in space. Rather, in order to maintain a constant temperature, $\partial_x(uT) = T\partial_x u$ is compensated by $\partial_y(vT) = T\partial_y v$ simply because the fluid is nondivergent. This simple example highlights the complications of examining heat flux divergence terms separately since they necessarily partly compensate because of mass convergence. By contrast, the individual advection terms that we have used here allow one to separate the contributions in the three spatial directions. This situation is confounded by the possibility of numerical roundoff errors in the flux approach. In a more recent paper, Jochum et al. (2005) have revisited their study with

another model but did not comment on the potential compensation between horizontal and vertical TIW advection in their new configuration. If their results still hold, it will be interesting to question if the mixed layer physics involved in our and their model configurations are responsible for the discrepancies.

We have seen that despite an overall agreement with observations in the mixed layer (important for predicting SST), the ocean model vertical velocities may be too small in the upper thermocline (Kennan and Flament 2000) and thus the vertical advection term (including TIW vertical advection) may be underestimated below, affecting heat budgets performed over depths deeper than that of the mixed layer. Resolution and mixing parameterizations are likely culprits, but studies with higher spatial resolution and slightly less lateral diffusion (Peter et al. 2006) also present such a bias. One key certainly resides in the parameterization of the lateral mixing operator as pointed out by Pezzi and Richards (2003) and Jochum et al. (2005). Also, in relation to this topic, estimates with higher-resolution models that resolve the TIWs' frontal areas should be designed since some studies (Sawyer 1996; Johnson 1996; Flament et al. 1996; Kennan and Flament 2000), suggest that very small scales and higher vertical speeds might be involved punctually in the frontal zone of the leading edge of the TIW.

Last, this study has shown that TIWs also modulate cooling by vertical mixing at the mixed layer base, tending to reduce it significantly on seasonal times scales. This effect is also very difficult to evaluate in observational studies. This argues for new observational studies designed to resolve the processes on the submesoscale.

Acknowledgments. We thank IRD for support and IDRIS NEC-SX5 for computer support. We also thank Sophie U. Cravatte for numerous and quite helpful comments. Thanks are also addressed to Matthieu P. La Languedep, M. Lengaigne, and Thomate Zegorgues. We also thank Dr. E. Firing and two anonymous reviewers for their comments and suggestions. Author S. Kennan was supported by NOAA Grant NA16GP2025.

APPENDIX A

Mixing and Mixed Layers

As discussed in Brainerd and Gregg (1995), there is a difference between the mixed layer and the mixing layer depths. In the model, the mixing layer is characterized by the depth over which the vertical eddy viscosity k is strong. This coefficient can show strong variations over a few model time steps, which gives a very variable mixing layer depth. Since we focus on the variability at TIW scales and not high-frequency variability such as the diurnal cycle, it is more appropriate to use the mixed layer depth rather than the mixing layer depth for the SST budget computation in Eq. (2) (Brainerd and Gregg 1995). In the model, the daily mixed layer is usually shallower than the mixing layer. Using the mixed layer depth thus results in diagnosing a negligible entrainment [term C in Eq. (2)], except in barrier layer regions (Vialard and Delecluse 1998b). In this case, however, the vertical eddy diffusion flux [term D in Eq. (2)] at the mixed layer base is strong since the mixing layer is deeper than the mixed layer. On the other hand, choosing the mixing layer depth for diagnosing the terms in Eq. (2) results in a negligible vertical diffusion in the equation, while the entrainment is strong. This is found when using integral mixed layer models such as in Jochum et al. (2004). Overall, the choice of mixed or mixing layers does not matter because the sum of entrainment and vertical diffusion remains identical in both cases.

APPENDIX B

Eddy and Mean Vertical Diffusion Decomposition

Contrary to temperature or currents, the vertical eddy viscosity k shows variations at the model time step (1.5 h), likely because it represents a large class of high-frequency energetic processes present in the upper tropical oceans. We tried to separate the vertical eddy diffusion term using an approach similar to Eq. (3) (using daily mean fields) but were unable to do so with limited error because k is highly variable over 1 day. Recalculating the mean vertical diffusion flux at the mixed layer base [term D in Eq. (2)] with daily outputs for the 1993–96 period gives an error of about 15%. The vertical diffusion $D_z(T)$ in Eq. (1) thus cannot be easily separated into mean and fluctuations. However, we have tried to assess qualitatively the effect of TIWs on the vertical diffusion term, because this term is strongly structured at TIW scales. We chose to compute the mean vertical diffusion flux $(1/h)(k_m \partial_z T_m)_{z=h}$ and to deduce the eddy-induced vertical diffusion flux by $(1/h)(k \partial T - k_m \partial_z T_m)_{z=h}$. By doing so, there is an error of about 15% in each of these terms, but their sum is exact. This is done in Eq. (6).

REFERENCES

Arakawa, A., 1972: Design of the UCLA general circulation model. Numerical simulation of weather and climate. Dept.

of Meteorology Tech. Rep. 7, University of California, 116 pp.

Baturin, N. G., and P. P. Niiler, 1997: Effects of instability waves in the mixed layer of the equatorial Pacific. *J. Geophys. Res.,* **102,** 27 771–27 793.

Bentamy, A., Y. Quilfen, F. Gohin, N. Grima, M. Lenaour, and J. Servain, 1996: Determination and validation of average wind fields from *ERS-1* scatterometer measurements. *Global Atmos. Ocean Syst.,* **4,** 1–29.

Blanke, B., and P. Delecluse, 1993: Variability of the tropical Atlantic Ocean simulated by a general circulation model with two different mixed layer physics. *J. Phys. Oceanogr.,* **23,** 1363–1388.

Brainerd, K. E., and M. C. Gregg, 1995: Surface mixed and mixing layer depths. *Deep-Sea Res.,* **42A,** 1521–1543.

Bryden, H. L., and E. C. Brady, 1989: Eddy momentum and heat fluxes and their effects on the circulation of the equatorial Pacific Ocean. *J. Mar. Res.,* **47,** 55–79.

Busalacchi, A. J., M. J. McPhaden, and J. Picaut, 1994: Variability in equatorial Pacific sea surface topography during verification phase of the TOPEX/Poseidon mission. *J. Geophys. Res.,* **99,** 24 725–24 738.

Chavez, F. P., P. G. Strutton, G. E. Friederich, R. A. Feely, G. C. Feldman, D. G. Foley, and M. J. McPhaden, 1999: Biological and chemical response of the equatorial Pacific Ocean to the 1997–1998 El Niño. *Science,* **286,** 2126–2131.

Chelton, D. B., F. J. Wentz, C. L. Gentemann, R. A. De Szoeke, and M. G. Schlax, 2000: Satellite microwave SST observations of transequatorial tropical instability waves. *Geophys. Res. Lett.,* **27,** 1239–1242.

——, and Coauthors, 2001: Observations of coupling between surface wind stress and sea surface temperature in the eastern equatorial Pacific. *J. Climate,* **14,** 1479–1498.

De Boyer Montégut, C., G. Madec, A. S. Fischer, A. Lazar, and D. Iudicone, 2004: Mixed layer depth over the global ocean: An examination of profile data and a profile-based climatology. *J. Geophys. Res.,* **109,** C12003, doi:10.1029/2004JC002378.

Flament, P., S. C. Kennan, R. Knox, P. P. Niiler, and R. Bernstein, 1996: The three-dimensional structure of an upper vortex in the tropical Pacific. *Nature,* **382,** 610–613.

Gibson, R., P. Kallberg, S. Uppala, A. Hernandez, A. Nomura, and E. Serrano, 1997: ERA description. Vol. 1, Re-analysis Project Report Series, ECMWF, Reading, United Kingom, 71 pp.

Halpern, D., R. A. Knox, and D. S. Luther, 1988: Observations of 20-day period meridional current oscillations in the upper ocean along the Pacific equator. *J. Phys. Oceanogr.,* **18,** 1514–1534.

Hansen, D., and C. Paul, 1984: Genesis and effect of long waves in the equatorial Pacific. *J. Geophys. Res.,* **89,** 10 341–10 440.

Harrison, D. E., 1996: Vertical velocities in the central tropical Pacific: A circulation model perspective for JGOFS. *Deep-Sea Res.,* **42B,** 753–778.

——, R. D. Romea, and S. H. Hankin, 2001: Central equatorial Pacific zonal currents. I: The Sverdrup balance, nonlinearity and tropical instability waves. Annual mean dynamics. *J. Mar. Res.,* **59,** 865–919.

Huffman, G. J., and Coauthors, 1997: The Global Precipitation Climatology Project (GPCP) Combined Precipitation Dataset. *Bull. Amer. Meteor. Soc.,* **78,** 5–20.

Jackett, D. R., and T. J. McDougall, 1995: Minimal adjustment of hydrographic data to achieve static stability. *J. Atmos. Oceanic Technol.,* **12,** 381–389.

Jochum, M., P. Manalotte-Rizzoli, and A. J. Busalacchi, 2004: Tropical instability waves in the Atlantic Ocean. *Ocean Modell.*, **7,** 145–163.

——, R. Murtugudde, R. Ferrari, and P. Manalotte-Rizzoli, 2005: The impact of horizontal resolution on the tropical heat budget in an Atlantic Ocean model. *J. Climate,* **18,** 841–851.

Johnson, E. S., 1996: A convergent instability wave front in the central tropical Pacific. *Deep-Sea Res.,* **43B,** 687–705.

Kennan, S. C., and P. Flament, 2000: Observations of a tropical instability vortex. *J. Phys. Oceanogr.,* **30,** 2277–2301.

Legeckis, R., 1977: Long waves in the eastern equatorial Pacific Ocean: A view from a geostationary satellite. *Science,* **197,** 1179–1181.

Lengaigne, M., G. Madec, C. Menkes, and G. Alory, 2003: Effect of isopycnal diffusion in the tropical Pacific Ocean. *J. Geophys. Res.,* **108,** 3345, doi:10.1029/2002JC001704.

Levitus, S., 1982: *Climatological Atlas of the World Ocean*. NOAA Prof. Paper 13, 173 pp. and 17 microfiche.

Lien, R.-C., M. J. McPhaden, and M. C. Gregg, 1996: High-frequency internal waves at 0°, 140°W and their possible relationship to deep-cycle turbulence. *J. Phys. Oceanogr.,* **26,** 581–600.

Lyman, J. M., D. B. Chelton, R. A. deSzoeke, and R. M. Samelson, 2005: Tropical instability waves as a resonance between equatorial Rossby waves. *J. Phys. Oceanogr.,* **35,** 232–254.

Madec, G., P. Delecluse, M. Imbard and C. Levy, 1999: OPA 8.1 Ocean general circulation model reference manual. Note du Pôle de Modélisation 11, Institut Pierre Simon Laplace, France, 91 pp.

Maes, C., G. Madec, and P. Delecluse, 1997: Sensitivity of an equatorial Pacific OGCM to the lateral diffusion. *Mon Wea. Rev.,* **125,** 958–971.

McCreary, J. P., and Z. Yu, 1992: Equatorial dynamics in a 2.5-layer model. *Progress in Oceanography,* Vol. 29, Pergamon, 61–132.

McPhaden, M. J., 1996: Monthly period oscillations in the Pacific North Equatorial Countercurrent. *J. Geophys. Res.,* **101,** 6337–6359.

Menkes, C., J.-P. Boulanger, A. J. Busalacchi, J. Vialard, P. Delecluse, M. J. McPhaden, E. Hackert, and N. Grima, 1998: Impact of TAO vs. ERS wind stresses onto simulations of the tropical Pacific Ocean during the 1993–1998 period by the OPA OGCM, Climatic Impact of Scale Interactions for the Tropical Ocean-Atmosphere System. *Euroclivar Workshop Report,* **13,** 46–48.

——, and Coauthors, 2002: A whirling ecosystem in the equatorial Atlantic. *Geophys. Res. Lett.,* **29,** 1553, doi:10.1029/2001GL014576.

Perigaud, C., 1990: Sea level oscillations observed with *Geosat* along the two shear fronts of the North Equatorial Countercurrents. *J. Geophys. Res.,* **95,** 7239–7248.

Peter, A. C., and Coauthors, 2006: A model study of the seasonal mixed layer heat budget in the equatorial Atlantic. *J. Geophys. Res.,* in press.

Pezzi, L. P., and K. J. Richards, 2003: Effects of lateral mixing on the mean state and eddy activity of an equatorial ocean. *J. Geophys. Res.,* **108,** 3371, doi:10.1029/2003JC001834.

Philander, G., and Coauthors, 1985: Long waves in the equatorial Pacific Ocean. *Eos, Trans. Amer. Geophys. Union,* **66,** 154–156.

——, W. J. Hurlin, and R. C. Pacanowski, 1986: Properties of long equatorial waves in models of the seasonal cycle in the tropical Atlantic and Pacific Oceans. *J. Geophys. Res.,* **91,** 14 207–14 211.

Qiao, L., and R. H. Weisberg, 1995: Tropical instability wave kinematics: Observations from the Tropical Instability Wave Experiment (TIWE). *J. Geophys. Res.,* **100,** 8677–8693.

Reynolds, R. W., and T. M. Smith, 1994: Improved global sea surface temperature analyses. *J. Climate,* **7,** 929–948.

Sawyer, M., 1996: Convergence and subduction at the North Equatorial Front. M.S. thesis, School of Ocean and Earth Science and Technology, University of Hawaii at Manoa, 92 pp.

Stevenson, J. W., and P. P. Niiler, 1983: Upper ocean heat budget during the Hawaii-to-Tahiti Shuttle Experiment. *J. Phys. Oceanogr.,* **13,** 1894–1907.

Swenson, M. S., and D. V. Hansen, 1999: Tropical Pacific Ocean mixed layer heat budget: The Pacific cold tongue. *J. Phys. Oceanogr.,* **29,** 83–91.

Tréguier, A.-M., O. Boebel, B. Barnier, and G. Madec, 2003: Agulhas eddy fluxes in a 1/6° Atlantic model. *Deep-Sea Res.,* **50,** 251–280.

Vialard, J., and P. Delecluse, 1998a: An OGCM study for the TOGA decade. Part I: Role of salinity in the physics of the western Pacific fresh pool. *J. Phys. Oceanogr.,* **28,** 1071–1088.

——, and ——, 1998b: An OGCM study for the TOGA decade. Part II: Barrier-layer formation and variability. *J. Phys. Oceanogr.,* **28,** 1089–1106.

——, C. Menkes, J.-P. Boulanger, P. Delecluse, E. Guilyardi, and M. McPhaden, 2001: A model study of the oceanic mechanisms affecting the equatorial SST during the 1997–98 El Niño. *J. Phys. Oceanogr.,* **31,** 1649–1675.

——, P. Delecluse, and C. Menkes, 2002: A modeling study of salinity variability and its effects in the tropical Pacific Ocean during the 1993–99 period. *J. Geophys. Res.,* **107,** 8005, doi:10.1029/2000JC000758.

——, C. Menkes, D. L. T. Anderson, and M. Balmaseda, 2003: Sensitivity of Pacific Ocean tropical instability waves to initial conditions. *J. Phys. Oceanogr.,* **33,** 105–121.

Wang, W., and M. J. McPhaden, 1999: The surface layer heat balance in the equatorial Pacific Ocean. Part I: Mean seasonal cycle. *J. Phys. Oceanogr.,* **29,** 1812–1831.

Weidman, P. D., D. L. Mickler, B. Dayyani Et, and G. H. Born, 1999: Analysis of Legeckis eddies in the near-equatorial Pacific. *J. Geophys. Res.,* **104,** 7865–7887.